Journal of Advanced Research in Micro and Nano Engineering

Journal homepage:
https://semarakilmu.com.my/journals/index.php/micro_nano_engineering/index
ISSN: 2756-8210

Characterization of Physical, Morphological and Mechanical Properties of Poly-Lactic Acid/Graphene (PLA/GNPs) Biopolymer Composites using Fused Deposition Modelling

Nurul Fatihah Ab Ghani[1], Wan Sharuzi Wan Harun[1,*], Abang Mohd Faadhillah Abang Ahmad[1], Muhamad Eri Iskandar Mohamad Sa'edi[1], Nur Shafiqah Omar[1]

[1] Faculty of Mechanical and Automotive Engineering Technology, Universiti Malaysia Pahang (UMP), 26600 Pekan, Pahang, Malaysia

ARTICLE INFO

Article history:
Received 1 August 2024
Received in revised form 13 September 2024
Accepted 19 October 2024
Available online 30 November 2024

Keywords:
Fused deposition modelling; mechanical properties; physical properties; microstructure; PLA; graphene

ABSTRACT

A hybrid biopolymer composite consisting of Poly-Lactic Acid/Graphene Nanoplatelets (PLA/GNPs) was formulated using double planetary mixer (DPM) and processed into granules and utilized as the feedstock for additive manufacturing (AM) of structures using the Fused Deposition Modelling (FDM) technique. The study aimed to investigate the influence of different weight percentages (1%, 3% and 5%) of graphene nanoplatelets (GNPs) on the physical, morphological and mechanical properties of the printed test samples. Differential Scanning Calorimetry (DSC) revealed the temperature ranges for the glass transition temperature (T_g) and crystallinity temperature (T_c) to be 61–63 °C and 112–140 °C, respectively. Additionally, it was observed that the presence of graphene in the polymer matrix led to a decrease in the melting temperature (T_m), with the sample containing 1 wt% of GNPs displaying the highest melting point. Furthermore, the density of the biopolymer composite increased as the weight percentage of GNPs increased. Microscopic examination of the samples revealed the presence of voids, waves and interlayer gaps in all compositions containing GNPs. These conditions were likely caused by inadequate material preparation and inaccurate printing parameter settings. In terms of mechanical properties, the highest tensile modulus observed was 1.29 GPa with 5 wt% GNPs, the highest flexural modulus was 5.17 GPa with 5 wt% GNPs and the highest compressive modulus was 10.073 GPa with 3 wt% GNPs. These results may be attributed to low homogeneity during the mixing process.

1. Introduction

Biopolymers offer diverse applications but encounter challenges with cost-effectiveness and upholding consistent quality, underscoring the necessity for continued research and cooperative projects. To effectively leverage on the environmental benefits linked to biopolymers, suitable waste management facilities is also called for [1,2]. Biopolymers are widely used for a wide range of

* *Corresponding author.*
E-mail address: sharuzi@ump.edu.my

https://doi.org/10.37934/armne.27.1.112132

purposes, such as packaging, medical equipment, textiles and clothing, agriculture, personal care products, food and green solutions [3,4]. They provide sustainable alternatives and help to solve problems related to healthcare, agriculture and the environment. Biopolymers typically have properties particularly biodegradability, renewable source, biocompatibility and environmental sustainability. As a biopolymer, PLA has garnered significant attention and is increasingly renowned for its renewable and sustainable properties, sourced from plants like corn or sugarcane. Alongside its favourable mechanical properties, biodegradability and biocompatibility, PLA is an appealing option for applications that prioritize eco-friendly alternatives to traditional plastics [5,6]. PLA, when its matrix gets incorporated with graphene, PLA-graphene polymer composites exhibit certain advantages. Two-dimensional carbon allotrope known as graphene exhibits extraordinary mechanical, electrical and thermal properties. It improves the composite's characteristics such as strength, conductivity, insulating qualities and thermal stability when integrated with PLA [7-9]. This composite could be applied in adaptive electronics, technology for energy storage and sensors, among other things.

3D printing is a rapid and straightforward manufacturing method capable of producing complex geometries that are challenging to create using conventional machining approaches. Various 3D printing methods, including Fused Deposition Modelling (FDM), Stereolithography (SLA) and Digital Light Processing (DLP), offer diverse techniques to fabricate objects with variety of materials and levels of complexity [10-12]. In FDM, a solid polymer is melted through heat and extruded under regulated pressure throughout the extrusion process. On the other hand, SLA and DLP use UV irradiation to locally cure photocurable polymers in specific areas. Another method known as Direct Ink Writing (DIW) creates structures by extruding droplets through a nozzle at a constant pressure [13]. The FDM printing method is extensively utilized in 3D printing due to its affordability in terms of equipment cost, which does not require large-scale manufacturing facilities. Additionally, FDM offers a wide range of material options, including diverse thermoplastics and ceramic filaments, offering versatility in material selection for different applications [14,15]. Due to its speed, FDM printing technology is preferable to other technologies since it allows CAD drawings to be converted into the end-product in a single step. It also provides excellent accuracy, with an estimated precision of 0.005 inches, which is accomplished by heating and layer upon layer extrusion of thermoplastic materials. FDM also makes it simple to scale the printed item without compromising accuracy, accommodating the requirements for manufacturing space [15]. The FFF printing method offers the versatility to utilize both rigid and flexible polymers, including materials like Polylactic acid (PLA) and Thermoplastic polyurethane (TPU). Furthermore, the incorporation of novel materials allowing fine-tuning of the properties of the 3D printed structures, enabling customization and optimization based on particular application specification [16].

The mixing process producing polymer composites entails blending several components to produce a homogeneous blend. Several techniques, including melt blending, solution blending, solid-state blending and in-situ polymerization, can be used to carry out this procedure [17,18]. These methods help to achieve the required material qualities and performance attributes by facilitating the dispersed distribution of fillers, reinforcing fibres, additives or other polymers inside the polymer matrix [16]. Melt-blending for polymer composites is normally ideal for thermoplastic materials. Thermoplastics are compatible with melt-blending techniques because they can repeatedly melt and solidify without suffering significant deterioration. Some common thermoplastics used in melt-blending for polymer composites include polyethylene (PE), polypropylene (PP), polystyrene (PS), polyethylene terephthalate (PET) and polyamide (PA) [19-23]. Additives, fillers or reinforcing agents can be effectively mixed with thermoplastics through melt-blending techniques to create composite materials with enhanced properties. Twin-screw extruders, single-screw extruders, mixing rolls and

internal mixers are some of the frequently used pieces of equipment [24-26]. The mixing efficiency, process speed and scalability of twin extruders may be better, but their cost and complexity are constrained. On the other hand, despite having a reduced throughput and mixing efficiency, planetary mixers excel in terms of providing better flexibility and compatibility with different thermoplastic polymer composites [24-26]. Twin extruder is commonly used by big industrial companies, but, small businesses organization based on 3D Printing technology could not afford such technology like twin extruder might opted to use planetary mixer for small batch of customed composite materials. When mixing a polymer composite, adding fillers to the polymer composites often aims to enhance its properties [27-29]. However, each mixture has a specific percolation threshold and exceeding it can result in either improvement or decline in properties, necessitating careful consideration for optimal composite performance [27-29].

In this present report, we demonstrate that mixing polymer composite using double planetary mixer would also result with the same enhanced material properties. We show PLA/GNPs composite characterizations and the optimizations of the material for additive manufacturing. FDM 3D printer was fed with granulated PLA/GNPs biopolymer composite of different filler weight percentage, fabricates samples for physical, mechanical and morphological characterization. The test result of the fabricated samples showing positive trends with little fluctuations. This suggests the existence of inconsistence or disturbance factors during the mixing process or printing process.

2. Materials and Methodology

2.1 Materials Preparation

Poly-Lactic Acid (PLA) in pellet form is purchase from Orinko Advanced Plastics Co., Ltd. Graphene Nanoplatelets (GNPs) in powder form is mixed with PLA with three different composition (1 wt %, 3 wt %, 5 wt%) using double planetary mixer (DPM). PLA/1GNPs, PLA/3GNPs and PLA/5GNPs refers to 1 wt %, 3 wt %, 5 wt% of GNPs. The DPM orbits on a common axis, two identical blades rotate on their own axes to transfer material. The blades move continually along the outside of the mixing vessel, scooping up material from the walls and transferring it inside. First, PLA is preheated at 200^{o}C for 1 hour. GNPs is then added according to mentioned composition which will make a total 500g composite. The mixing time is 30-60 minutes with low speed approximately 25% from machine's top speed. The double planetary mixer is a crucial production tool for the bulk mixing of solid propellants because it offers sufficient bulk circulation and effective homogenization for particularly viscous materials [30,31]. The clearance and helix angle of the blades, which are essential parts of a double planetary mixer, have a big impact on both power usage and mixing effectiveness [31,32]. The biopolymer composite produced in solidified homogenous batter which then going through several manual process steps to reduce its size into granules not less than 2mm to make it suitable for Fused Deposition Modelling (FDM) feedstock.

2.2 3D Model Slicing

SOLIDWORKS 2022 is used to design the 3D model of dog-bone shape sample for the tensile test, cylindrical sample for the compression test and rectangular sample for bending testing. The 3D Model then sliced and saved into. stl format using Simplify3D as shown in Figure 2, Figure 3 and Figure 4.

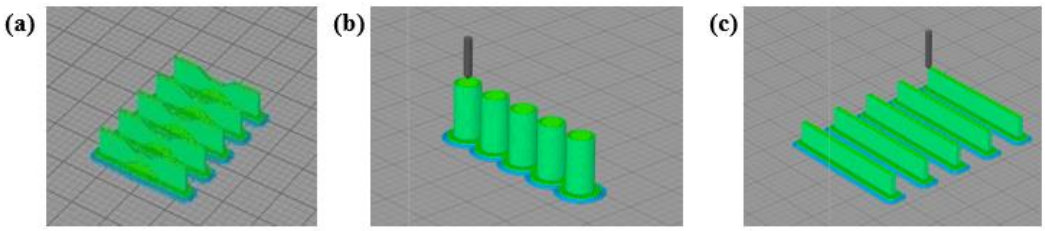

Fig. 1. Sliced model (a) Tensile samples (b) Compression samples (c) Flexural samples

2.3 Fused Deposition Modelling

The FDM machine used is PIOCREAT G5 Industrial FGF Pellets 3D Printer. 15 samples were produced at which 5 samples per set for three types of mechanical tests. Table 1 displays the FDM printing parameter settings used for samples fabrication.

Table 1
Fused deposition modelling (FDM) printing parameter

Parameter	Values
Nozzle Diameter(mm)	0.4
Layer thickness (mm)	0.2
Solid layers	Every 3 layer (top and bottom)
Bed temperature (°C)	60-70
Nozzle Temperature (°C)	200-220
Printing speed (mm/s)	60
Flowrate (%)	200
Internal fill pattern	Triangular
External fill pattern	Rectilinear
Infill percentage	100 %

2.4 Physical Characterization

A vernier calliper with a precision of 0.05mm was used to measure the dimensions of the printed samples. Volume of the samples are calculated from the dimensions obtained. Meanwhile, in addition of D790 flexural samples (80 mm x 10 mm x 4 mm), another 5 samples based on ASTM D2240 (are printed for density measurement. Measuring cylinder and digital balance are used to study the samples' density. For a precise result, three readings were taken for each sample. The experimental values of dimensions measurement, density is compared with theoretical value. The differential scanning calorimetry (DSC) analysis was performed to analyse the thermal properties of PLA/1GNPs, PLA/3GNPs and PLA/5GNPs. 5mg of each composition is analysed using DSC-8000 in the temperature range 25°C to 270°C with heating/cooling rate 10°C /min under nitrogen atmosphere at 50ml/min. The glass transition temperature (T_g), crystallinity temperature (T_c) and melting temperature (T_m) are studied from the DSC graph obtained.

2.5 Mechanical Characterization

Tensile test was performed using Instron 5900 Universal Testing Machine at crosshead speed 5mm/min using ASTM D638-IV standard. Compression testing was done using Instron 3369Q Universal Testing Machine with sample that follows ASTM D695-15. Compressive load used is 5 mm/min with compression percentage at 25% from original condition. With similar machine, flexural test sample follows ASTM D790 was tested with bending load at speed rate of 1 mm/min.

2.6 Morphological Characterization

Using an optical microscope (OM), the fractured surface's morphology was investigated. Detailed images of the sections were taken using a Zoom Stereo Microscope (SOPTOP), as shown in Figure 2. This facilitated the examination of the macro-morphologies of the damaged surfaces and revealed details regarding the morphological structure of the 3D-printed materials. The OM images enabled for the evaluation of interactions between each layer and the detection of imperfections that could affect the mechanical properties of the printed samples because FDM technology operates on a layer-by-layer basis [33].

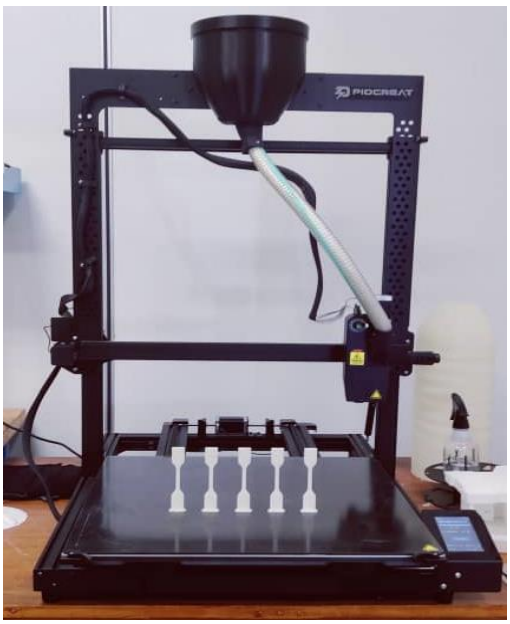

Fig. 2. G5 industrial FGF pellets 3D printer

3. Results and Discussion

3.1 Physical Properties

3.1.1 Dimensional accuracy

The dimensional accuracy of ASTM D2240 samples and ASTM D790 samples show consistent trend for length and width measurement where the percentage value increase with the increment of GNPs weight percentage. However, thickness measurement shows inconsistency when the accuracy percentage drops for PLA/3GNPs. Trend summary can be seen in Figure 3. Error percentage is calculated based on equation below:

$$\text{Error } \% = \frac{|Nominal\ value - Actual\ value|}{Nominal\ Value} \times 100 \quad (1)$$

$$Accuracy\ \% = 100\% - Error\ \% \quad (2)$$

Table 2 and Table 4 shows details of measurements taken from three samples fabricated for each standard. An average value is calculated which then compared with theoretical value to get an error percentage. Smallest error percentage recorded is 2.66% for PLA/5GNPs using ASTM D2240 standard samples in Table 3 while the highest error percentage recorded is 19.25% at PLA/1NPs composition for sample ASTM D790 in Table 5.

Table 2
Dimension comparison for ASTM D2240 samples of PLA/1GNPs, PLA/3GNPs and PLA/5GNPs

Dimension <nominal>	Length (mm) <30mm>					Width (mm) <7mm>					Thickness (mm) <6.4mm>				
Sample	1	2	3	Average	σ	1	2	3	Average	σ	1	2	3	Average	σ
PLA/1GNPs	30.60	30.40	30.50	30.50	0.1000	7.40	7.15	7.30	7.28	0.0866	6.80	6.65	6.85	6.77	0.0000
PLA/3GNPs	30.40	30.25	30.25	30.30	0.1258	7.15	7.00	7.10	7.08	0.0764	6.85	6.90	6.65	6.80	0.0289
PLA/5GNPs	30.25	30.25	30.25	30.25	0.1041	7.00	6.95	7.00	6.98	0.1323	6.55	6.6	6.55	6.57	0.0289

Table 3
Percentage error of ASTM D2240 measured dimensions

Material	Theoretical Length (mm)	Sample Length (mm)	Error (%)	Theoretical Width (mm)	Sample Width (mm)	Error (%)	Theoretical Thickness (mm)	Sample Thickness (mm)	Error (%)
PLA/1GNPs	30.00	30.50	1.67	7.00	7.28	4.00	6.40	6.77	5.78
PLA/3GNPs	30.00	30.30	1.00	7.00	7.08	1.14	6.40	6.80	6.25
PLA/5GNPs	30.00	30.25	0.83	7.00	6.98	0.86	6.40	6.57	2.66

Table 4
Dimension comparison for ASTM D790 samples of PLA/1GNPs, PLA/3GNPs and PLA/5GNPs

Dimension <nominal>	Length (mm) <80mm>					Width (mm) <10mm>					Thickness (mm) <4mm>				
Sample	1	2	3	Average	σ	1	2	3	Average	σ	1	2	3	Average	σ
PLA/1GNPs	80.30	80.55	80.50	80.45	0.1323	10.15	10.15	10.15	10.15	0.0577	4.70	4.85	4.75	4.77	0.0866
PLA/3GNPs	80.50	80.50	80.40	80.47	0.0764	10.20	10.15	10.20	10.18	0.0289	4.50	4.50	4.45	4.48	0.0866
PLA/5GNPs	80.95	80.80	80.80	80.85	0.0000	10.10	10.10	10.20	10.13	0.0289	4.45	4.45	4.60	4.50	0.0577

Table 5
Percentage error of ASTM D790 samples measured dimensions

Material	Theoretical Length (mm)	Sample Length (mm)	Error (%)	Theoretical Width (mm)	Sample Width (mm)	Error (%)	Theoretical Thickness (mm)	Sample Thickness (mm)	Error (%)
PLA/1GNPs	80.00	80.45	0.56	10.00	10.15	1.50	4.00	4.77	19.25
PLA/3GNPs	80.00	80.47	0.59	10.00	10.18	1.80	4.00	4.48	12.00
PLA/5GNPs	80.00	80.85	1.07	10.00	10.13	1.30	4.00	4.50	12.50

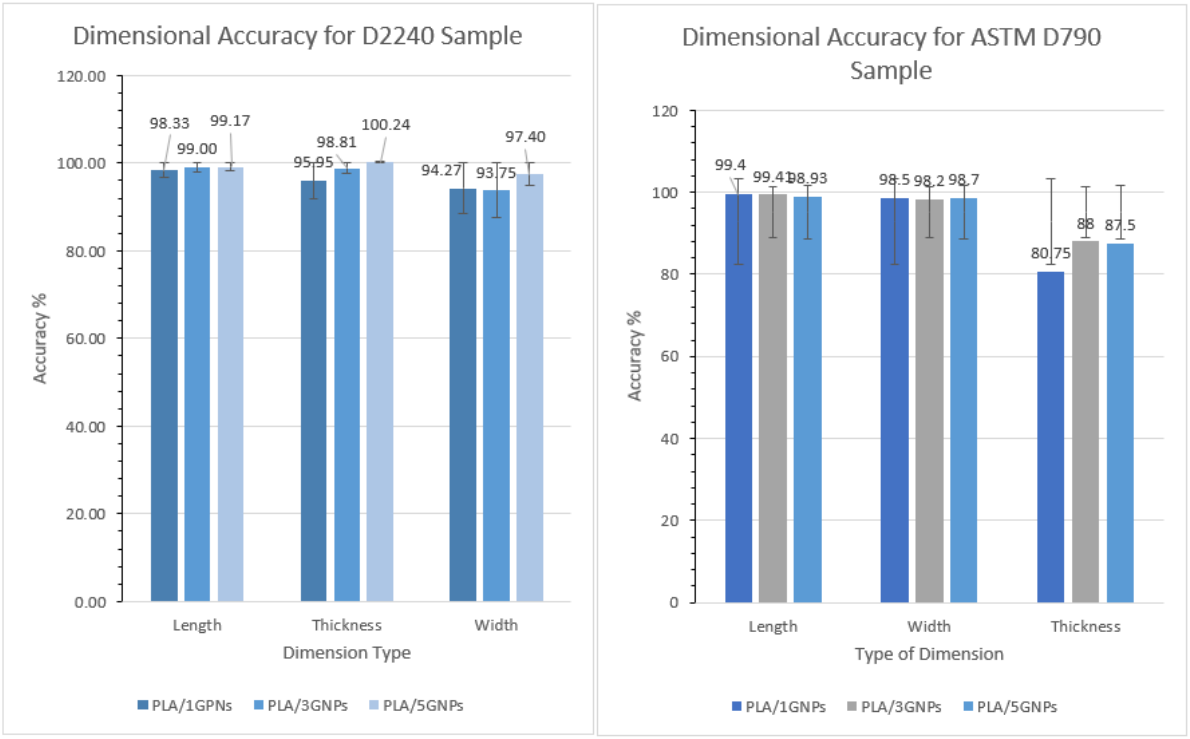

Fig. 3. Dimensional accuracy comparison between PLA/1GNPs, PLA/3GNPs and PLA/5GNPs for (a) ASTM D2240 sample (b) ASTM D790 sample

Based on Table 5 and Figure 3, sample D790 (ASTM D790 testing), the dimensional accuracy of the 3D printed PLA/GNPs composites was well-maintained across different weight percentages of GNPs. In the dimensional accuracy data obtained using ASTM D790 for the PLA/GNPs composites, the average length measurements for PLA/1GNPs, PLA/3GNPs and PLA/5GNPs are approximately 80.45 mm, 80.47 mm and 80.85 mm, respectively. The average width measurements for the same composites are approximately 4.77 mm, 4.48 mm and 4.50 mm, respectively. For the thickness dimension, the average measurements are approximately 10.15 mm, 10.18 mm and 10.13 mm for PLA/1GNPs, PLA/3GNPs and PLA/5GNPs, respectively. The standard deviation values for length, width and thickness dimensions are relatively small, with maximum values of 0.1323 mm, 0.0577 mm and 0.0866 mm, respectively. Similarly, the standard error values are also small, with maximum values of 0.0764 mm, 0.0333 mm and 0.0500 mm for length, width and thickness dimensions, respectively. These small standard deviation and standard error values indicate good dimensional stability and consistency in the 3D printed PLA/GNPs composites.

On the other hand, for the dimensional accuracy data obtained using ASTM D2240, the average length measurements for Sample 1, Sample 2 and Sample 3 are approximately 30.50 mm, 30.30 mm and 30.25 mm, respectively. The average width measurements for the same samples are approximately 7.28 mm, 7.08 mm and 6.98 mm, respectively. For the thickness dimension, the average measurements are approximately 6.77 mm, 6.80 mm and 6.57 mm for Sample 1, Sample 2 and Sample 3, respectively. The standard deviation values for length, width and thickness dimensions are relatively small, with maximum values of 0.1000 mm, 0.1323 mm and 0.0866 mm, respectively. Similarly, the standard error values are also small, with maximum values of 0.0577 mm, 0.0764 mm and 0.0500 mm for length, width and thickness dimensions, respectively.

These small standard deviation and standard error values in the ASTM D2240 data indicate good dimensional stability and consistency for the samples tested. Overall, the dimensional accuracy data

using ASTM D790 demonstrates the consistent and precise measurements of length, width and thickness in the PLA/GNPs composites, meeting the requirements of various applications. However, the data obtained using ASTM D2240 is not appropriate for dimensional accuracy assessments and using other suitable standard test methods is recommended for more reliable results.

3.2 Density

Two samples were printed using ASTM D790 and ASTM D2240 for each composition. Next, the average value of mass and volume were measured from 6 different samples with the same printing parameter. Figure 4 shows the average density of the samples for each composition.

$$Density = \frac{Mass}{Volume} \tag{3}$$

To compare with experimental density values is calculated using formula by Gauss *et al.,* [5] while theoretical density value of biopolymer composites is calculated as in Table 6.

Table 6
Theoretical density of neat PLA, neat GNP and PLA/GNPs biopolymer composite

Material	Density Formula	Density (g/cm^3)
PLA	-	1.25
GNP	-	2.25
PLA/1GNPs	(0.99 x 1.25) + (0.01 x 2.25)	1.26
PLA/3GNPs	(0.97 x 1.25) + (0.03 x 2.25)	1.28
PLA/5GNPs	(0.95 x 1.25) + (0.05 x 2.25)	1.30

Table 7 and Table 8 shows details measurement of mass and volume for each composition to obtained average readings for comparison with theoretical value. The average experimental density for each composition for both sample standard ASTM D790 and D2240 are same where the value is 1.23g/ml, 1.28 g/ml and 1.29 g/ml.

Table 7
Weight, volume and density of ASTM D2240 samples

Sample	1		2		3		Average		Density (g/ml)	Standard Deviation, σ		
	Mass (g)	Volume (ml)	Mass (g)	Volume (ml)	Mass (g)	Volume (ml)	Mass (g)	Volume (ml)		Mass (g)	Volume (ml)	Density (g/ml)
PLA/1GNPs	1.72	1.4	1.73	1.4	1.72	1.4	1.72	1.4	1.23	0.0058	0.000	0.0041
PLA/3GNPs	1.65	1.3	1.67	1.3	1.66	1.3	1.66	1.3	1.28	0.0100	0.000	0.0077
PLA/5GNPs	1.54	1.2	1.58	1.2	1.53	1.2	1.55	1.2	1.29	0.0265	0.000	0.0220

Table 8
Weight, volume and density of ASTM D790 samples

Sample	1		2		3		Average		Density (g/ml)	Standard Deviation, σ		
	Mass (g)	Volume (ml)	Mass (g)	Volume (ml)	Mass (g)	Volume (ml)	Mass (g)	Volume (ml)		Mass (g)	Volume (ml)	Density (g/ml)
PLA/1GNPs	1.72	1.4	1.73	1.4	1.72	1.4	1.72	1.4	1.23	0.0866	0.1155	0.0127
PLA/3GNPs	1.65	1.3	1.67	1.3	1.66	1.3	1.66	1.3	1.28	0.0709	0.1000	0.0133
PLA/5GNPs	1.54	1.2	1.58	1.2	1.53	1.2	1.55	1.2	1.29	0.0153	0.0000	0.0045

Based on Table 9, the accuracy of density measurement achieves 100% for PLA/3GNPs. Trend of density accuracy can be seen in Figure 4.

Table 9
Comparison of theoretical density vs experimental density for ASTM D2240 and ASTM D790 samples, error percentage of PLA/1GNPs, PLA/3GNPs and PLA/5GNPs

Material	Theoretical Density (g/cm3)	Density Sample ASTM D2240 (g/cm3)	Error (%)	Density Sample ASTM D790 (g/cm3)	Error (%)
PLA/1GNPs	1.26	1.23	2.38	1.23	2.38
PLA/3GNPs	1.28	1.28	0.00	1.28	0.00
PLA/5GNPs	1.30	1.29	0.77	1.29	0.77

The accuracy values for density measurements using ASTM D2240 for all three materials (PLA/1GNPs, PLA/3GNPs and PLA/5GNPs) are quite high, with values close to 100%. This indicating that the density measurements are very close to the actual or expected density of the materials. The error percentages are relatively low, ranging from 0.00% to 0.02%. The standard deviation values for the density measurements using ASTM D2240 are also very small, with values of 0.0041, 0.0077 and 0.0220 for PLA/1GNPs, PLA/3GNPs and PLA/5GNPs, respectively. Low value standard deviation indicate that the density measurements are precise and consistent for each material.

Like ASTM D2240, the accuracy values for density measurements using ASTM D790 for all three materials (PLA/1GNPs, PLA/3GNPs and PLA/5GNPs) are quite high, with values close to 100%. The error percentages for ASTM D790 density measurements are also very low, ranging from 0.08% to 0.09%. This indicates that the density measurements using ASTM D790 are highly accurate and have minimal deviation from the true density values. Interestingly, the standard deviation values for the density measurements using ASTM D790 are all zero (0.0000). A standard deviation of zero suggests that all the measurements for each material have the same value, indicating perfect precision and no variability in the data points.

The data presented in the tables indicate that the density measurements for the materials using both ASTM D2240 and ASTM D790 are highly accurate and precise, with very small errors and standard deviations. The consistency and accuracy of the density measurements suggest that both testing methods are reliable and well-suited for measuring the density of the materials. The results also show that adding varying percentages of GNPs to the PLA material does not significantly affect the accuracy and precision of the density measurements, as indicated by the similar error and standard deviation values for PLA/1GNPs, PLA/3GNPs and PLA/5GNPs in both sample tests. Overall, the data trend demonstrates that the density measurements for the materials are highly reliable and the use of ASTM D2240 and ASTM D790 methods yields accurate and consistent results, providing confidence in the density values obtained for the different materials.

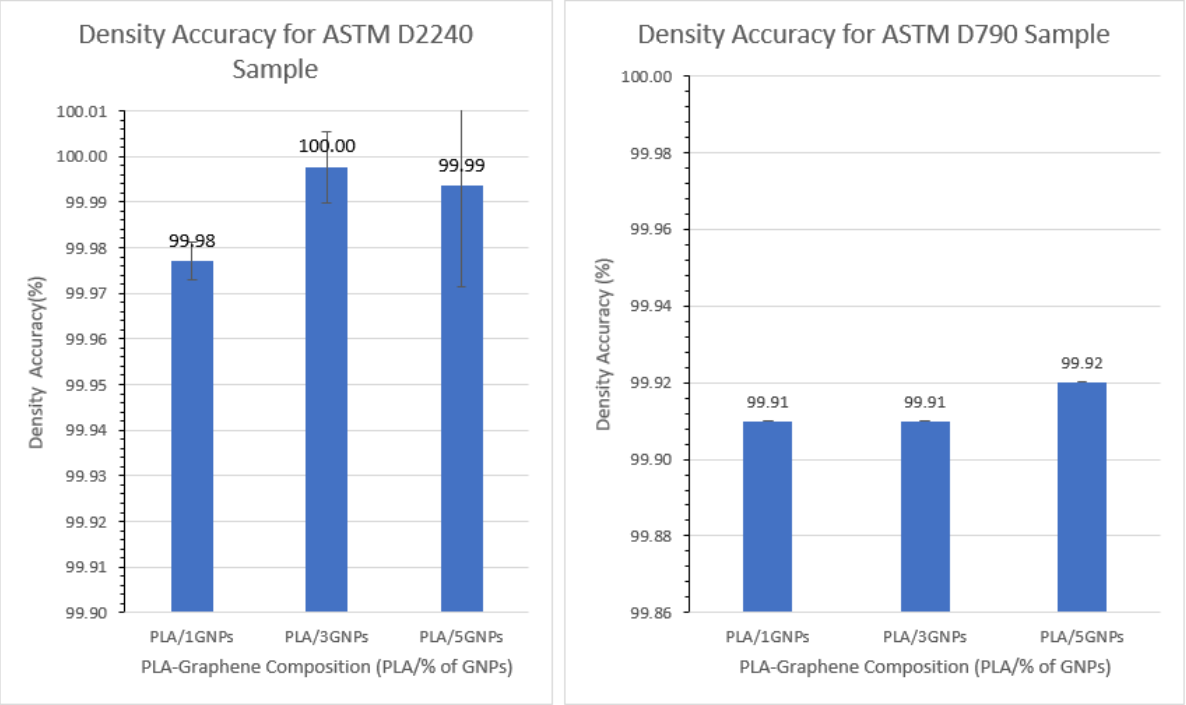

Fig. 4. Density accuracy comparison between PLA/1GNPs, PLA/3GNPs and PLA/5GNPs for (a) D2240 sample (b) D790 sample

3.3 Differential Scanning Calorimetry (DSC)

The glass transition is the process by which materials change when the temperature rises from a stiff or brittle condition to a more fluid or rubbery one [6,7]. The process of crystallisation, in contrast, is a transitional phase between melting and the glassy state in which the molecules gather enough energy to reorganise themselves into a crystalline structure [6,7]. The glass transition temperature (Tg) and crystallinity temperature (Tc) reported on the DSC graph were found to be between 61 and 63 °C and 112-140 °C, respectively. The analysis revealed that adding graphene to the PLA composite resulted in an increase in crystallinity temperature while just slightly lowering the glass transition temperature. The DSC measurements also showed that the addition of graphene to the matrix made the melting temperature (Tm) to drop. This decrease in Tm can be attributed to the thermoplastic matrix's and graphene's poor interfacial adhesion, which makes it simpler for intermolecular chains to break. Notably, the sample with the highest melting point was the one with 1% filler as stated in Table 10. Overview of DSC graph comparison of PLA/1GNPs, PLA/3GNPs and PLA/5GNPs can be seen in Figure 6.

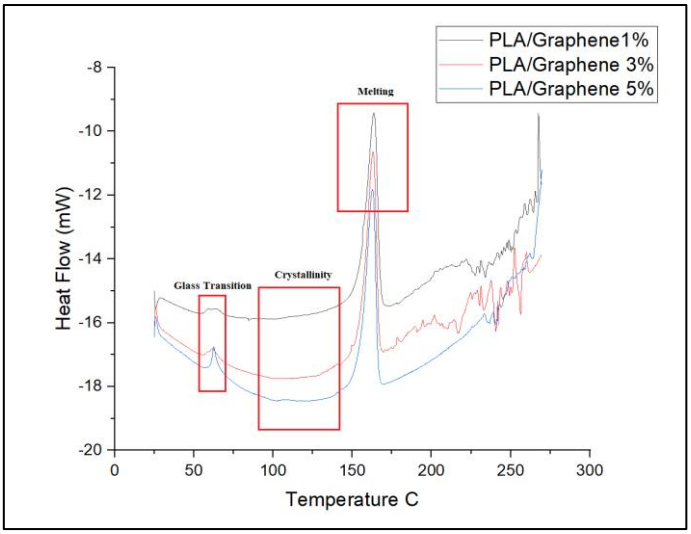

Fig. 5. DSC graph comparison of PLA/1GNPs, PLA/3GNPs and PLA/5GNPs

Table 10
Thermal properties of PLA/1GNPs, PLA/3GNPs and PLA/5GNPs

Sample	Glass Transition Temperature, T_g (°C)	Crystallinity Temperature, T_c (°C)	Melting Temperature, T_m (°C)
PLA/1GNPs	63.74	112	163.66
PLA/3GNPs	61.52	131	163.083
PLA/5GNPs	62.58	140	162.80

3.4 Mechanical Properties

Table 11 shows the Image of samples before and after tensile, compression and flexural testing.

Table 11
Image of samples before and after tensile, compression and flexural testing

Mechanical Test	Before	After
Tensile		
Compression		
Flexural		

3.5 Tensile Test

The Modulus represents the stiffness or rigidity of the material. Observation of trend in Figure 6(a), the modulus values for PLA/0GNPs, PLA/1GNPs and PLA/3GNPs fall within the range of approximately 1000 MPa to 1300 MPa. However, the Modulus for PLA/5GNPs is missing for some samples. Among the compositions, PLA/1GNPs exhibits the highest average Modulus of 1237.62 MPa, whereas PLA/0GNPs shows the lowest average Modulus of 1003.93 MPa.

Tensile stress at tensile strength shown in Figure 6(b) indicates the maximum stress the material can withstand before breaking during a tensile test. We observe variations in tensile stress at tensile strength values for each PLA/GNP composition. PLA/1GNPs exhibits the highest average tensile stress at tensile strength of 74.31 MPa, followed by PLA/3GNPs (71.63 MPa) and PLA/5GNPs (65.45 MPa). In contrast, PLA/0GNPs shows the lowest average tensile stress at tensile strength of 30.17 MPa. The trend shows that in terms of tensile Young's modulus and tensile stress at tensile strength, the composition of PLA/GNPs has a percolation threshold at 1 wt% graphene nanoplatelets. At concentrations exceeding the percolation threshold, metallic or carbon-based fillers can offer additional benefits, including enhanced thermal and electrical conductivity or vice-versa [27-29].

Figure 6(c) shows a variation in tensile stress at Break values among the PLA/GNP compositions. PLA/3GNPs demonstrates the highest average tensile stress at break of 44.38 MPa, followed by PLA/1GNPs (34.44 MPa) and PLA/5GNPs (37.61 MPa). In comparison, PLA/0GNPs has the lowest average tensile stress at break of 21.15 MPa.

Displacement at break represents the amount of elongation or deformation the material undergoes before breaking during the tensile test. For all PLA/GNP compositions, the displacement at break values is generally low, indicating that the materials exhibit a brittle behaviour with limited deformation before breaking. The average displacement at break ranges from approximately 0.59 mm for PLA/5GNPs to 4.80 mm for PLA/0GNPs which can be seen in Figure 6(d).

The addition of GNPs (Graphene Nanoplatelets) to PLA resulted in improvements in the mechanical properties, particularly the Young's modulus, tensile stress at tensile strength and tensile stress at break. Among the different compositions, PLA/1GNPs consistently exhibited the highest average values for these properties. However, the displacement at break values for all PLA/GNP compositions remained relatively low, suggesting that the materials tended to be brittle and underwent limited deformation before breaking.

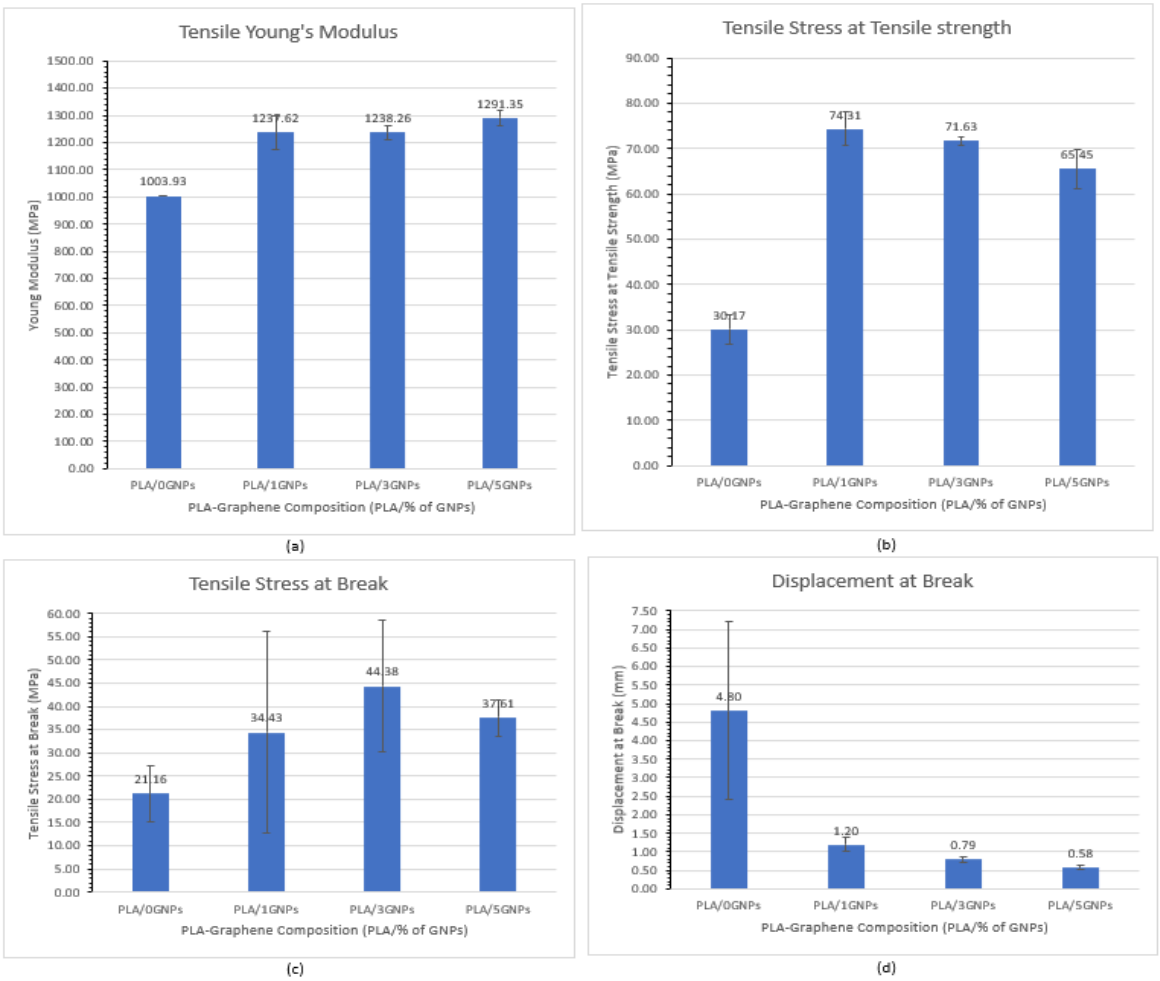

Fig. 6. Tensile test (a) Young's Modulus (b) Tensile stress at tensile strength (c) Tensile stress at break (d) Displacement at break

3.6 Compression Test

The compressive modulus (Automatic Young's) in Figure 7(a) represents the material's stiffness and resistance to deformation under compression. The data indicate that the incorporation of GNPs resulted in a significant increase in compressive modulus. PLA/1GNPs showed the highest average compressive modulus of 9766.314 MPa, followed by PLA/3GNPs (10073.056 MPa) and PLA/5GNPs (9376.636 MPa). This trend indicates that GNPs effectively reinforced the PLA matrix, leading to improved structural integrity and resistance to compression.

Figure 7(b) shows the compressive stress at maximum force represents the maximum stress the material can withstand before failure under compression, while the compressive strain (displacement) at maximum force represents the corresponding strain or deformation at this point. The data reveal that the compressive stress at maximum force increased with increasing GNP content. PLA/3GNPs exhibited the highest average compressive stress at maximum force (98.956 MPa), followed by PLA/5GNPs (82.714 MPa) and PLA/1GNPs (86.054 MPa). This suggests that GNPs played a crucial role in enhancing the compressive strength of the PLA composites. Interestingly, the compressive strain at maximum force remained relatively constant at approximately 0.02 mm/mm for all PLA/GNP compositions. This indicates that the addition of GNPs did not significantly affect the material's ductility or its ability to undergo deformation before failure under compressive loading.

The compressive displacement at maximum force represented in Figure 7(c) shows the amount of deformation the material undergoes at the point of maximum compressive force. The data show that the compressive displacement at maximum force is consistent across all PLA/GNP compositions, indicating that the presence of GNPs did not influence this parameter significantly.

Among the different PLA/GNP compositions, PLA/3GNPs displayed the highest average compressive stress at maximum force, suggesting that an optimal GNP loading was achieved at 3%wt. Both PLA/1GNPs and PLA/5GNPs exhibited competitive compressive stress at maximum force values, indicating the potential of GNPs as effective reinforcement agents for PLA composites. The data trend shows in Figure 7(d) given the result that for compressive test, the percolation threshold is at 3 wt% of graphene nanoplatelet, but further experimental with wider variables is needed to support the theory [27-29].

The observed improvements in the compressive properties of the PLA/GNP composites can be attributed to several factors. Firstly, the addition of graphene nanoplatelets (GNPs) resulted in enhanced stiffness, leading to an increase in the compressive, modulus. This improved stiffness made the materials more resistant to deformation and better equipped to withstand compressive loads.

Secondly, the uniform dispersion of GNPs within the PLA matrix played a crucial role in enhancing the compressive performance. The efficient distribution of GNPs allowed for effective stress transfer and load distribution throughout the material, ensuring that the compressive forces were evenly distributed and reducing the risk of localized failures.

Moreover, the strong interfacial interaction between the GNPs and the PLA matrix contributed significantly to the enhanced compressive properties. The strong adhesion between the GNPs and PLA matrix facilitated efficient stress transfer from the polymer matrix to the GNPs, reinforcing the material and leading to improved compressive stress at maximum force.

Overall, the combination of enhanced stiffness, efficient load transfer and strong interfacial interaction resulting from the addition of GNPs led to substantial improvements in the compressive behaviour of the PLA composites. These findings highlight the potential of PLA/GNP composites as high-performance materials for applications requiring excellent compressive strength and stability. Further research and optimization of the GNPs' content, distribution and mixing parameter optimization could open even more opportunities for the development of advanced composites with tailored compressive properties for specific industrial applications.

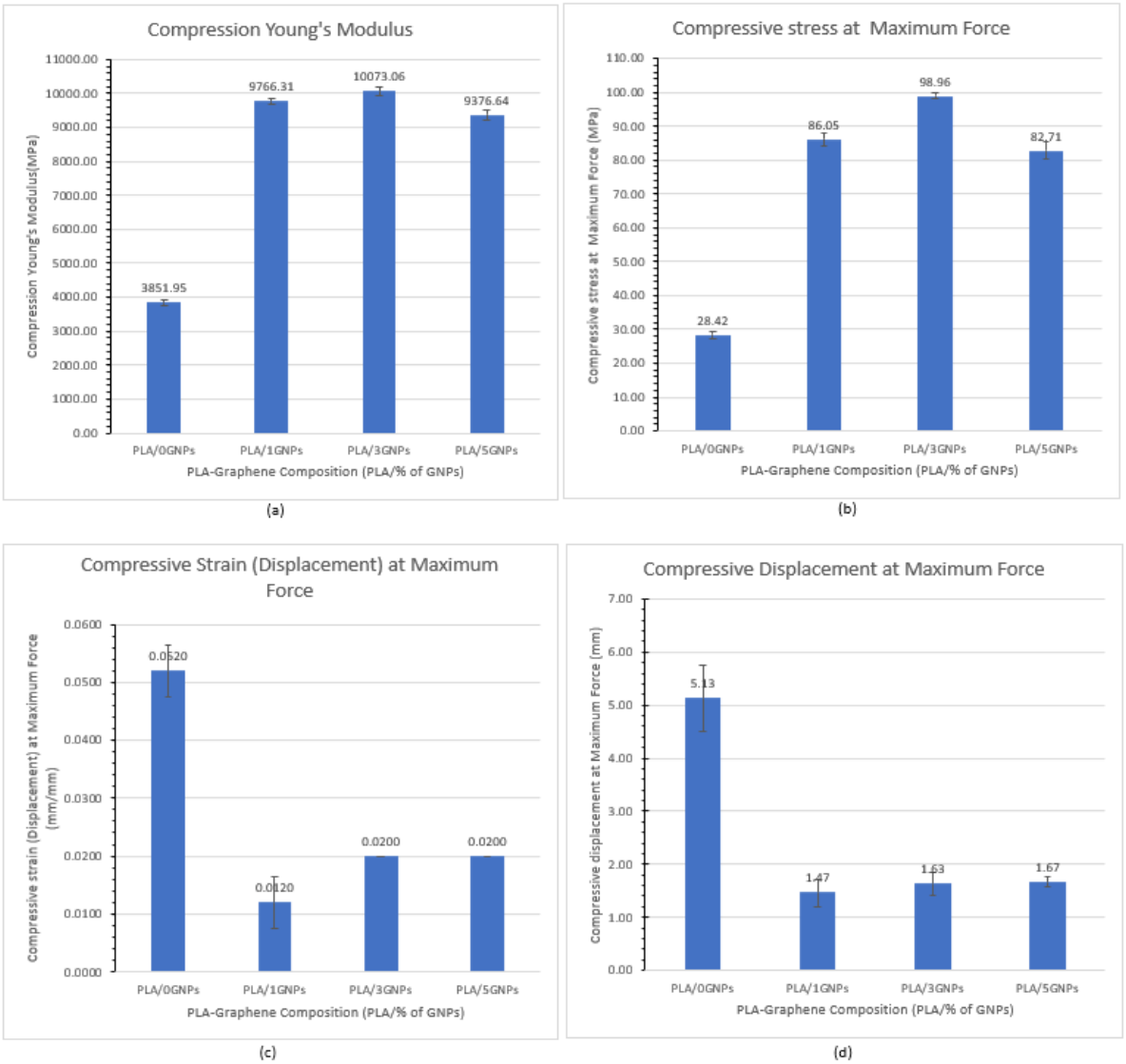

Fig. 7. Compression test (a) Young's Modulus (b) Compressive stress at maximum force (c) Compressive strain (displacement) at maximum force (d) Compressive displacement at maximum force

3.7 Flexural Test

The Modulus in Figure 8(a), which represents the stiffness of the material, increases with the addition of GNPs. PLA/1GNPs exhibits the highest average modulus (4930.29 MPa), followed by PLA/5GNPs (5166.03 MPa), PLA/3GNPs (4484.92 MPa) and PLA/0GNPs (2233.23 MPa). This suggests that incorporating GNPs enhances the composite's rigidity.

The Flexural stress at tensile strength which can be seen in Figure 8(b), indicating the material's maximum stress during the test, is also influenced by the addition of GNPs. PLA/1GNPs shows the highest average Flexural stress (119.50 MPa), followed by PLA/5GNPs (38.44 MPa), PLA/3GNPs (79.67 MPa) and PLA/0GNPs (38.29 MPa). This demonstrates that GNPs improve the material's strength in the flexural test.

The flexural displacement, which represented by graph in Figure 8(c), the material's deformation before breaking, is lower in PLA/5GNPs (5.29 mm) compared to PLA/0GNPs (6.68 mm), PLA/3GNPs

(6.50 mm) and PLA/1GNPs (6.80 mm). This indicates that the addition of GNPs results in a more rigid composite with limited deformation capacity.

The flexural strain, showing in Figure 8(d) shown the percentage elongation or deformation before breaking, follows a similar trend. PLA/5GNPs exhibits the lowest average Flexural strain (3.10%), followed by PLA/0GNPs (3.92%), PLA/3GNPs (3.81%) and PLA/1GNPs (3.98%). This further confirms that PLA/5GNPs is relatively more rigid with reduced deformation.

In summary, the data highlights that incorporating GNPs into PLA composites enhances their stiffness, strength and reduces deformation under flexural stress. PLA/1GNPs and PLA/5GNPs consistently display the most significant improvements in these mechanical properties, making them promising candidates for applications requiring high rigidity and strength. However, it is essential to consider specific application requirements and trade-offs when choosing the appropriate weight percentage of GNPs for optimal composite performance. Further investigation and testing may be needed to fine-tune the composite properties for specific engineering and industrial applications.

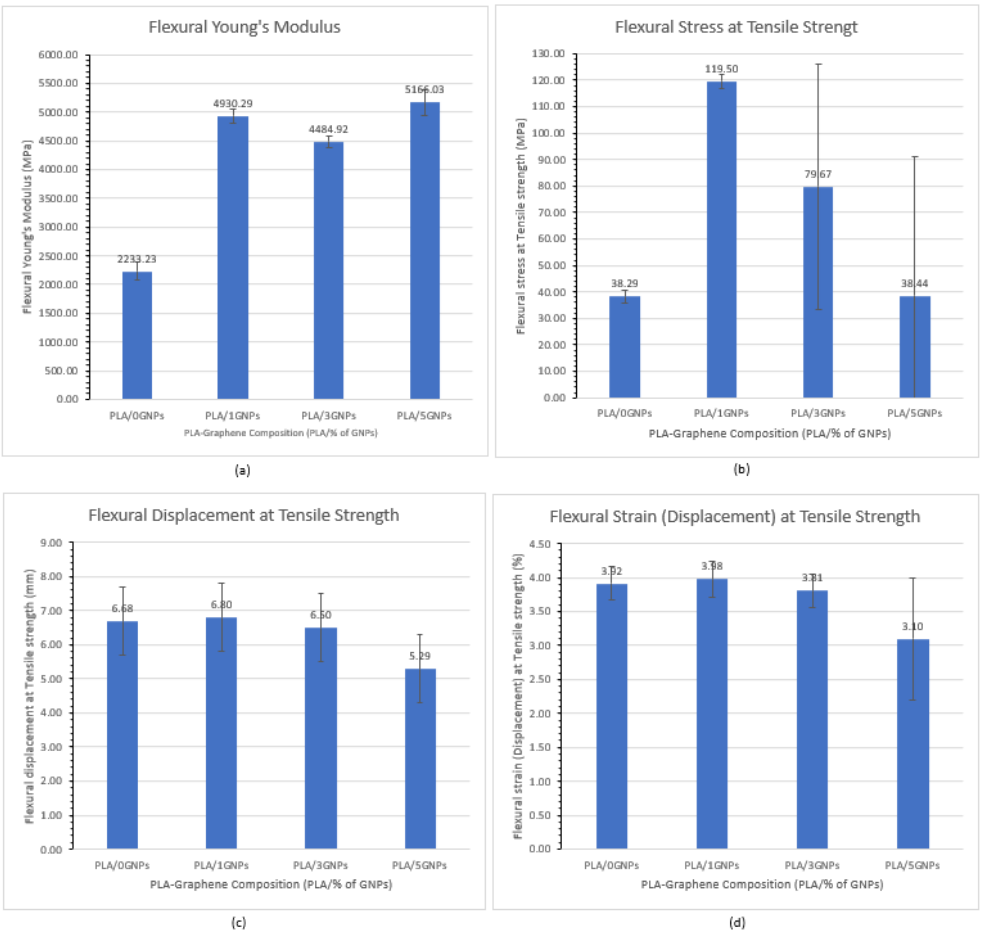

Fig. 8. Flexural test (a) Young Modulus (b) Flexural stress at tensile strength (c) Flexural displacement at tensile strength (d) Flexural strain (displacement) at tensile strength

3.8 Morphology - Microstructure Observation

The optical microscope images of the fractured cross-section of the four samples with:

i. PLA/1GNPs
ii. PLA /3GNPs
iii. PLA/5GNPs
iv. Neat PLA that undergone a tensile test are shown in Figure 10.

From the microstructure image obtained, indication of brittle failure is found. Fracture surface is seen at the breaking point cross section of the test samples. The fracture pattern shows that the material failing from the midsection of the samples parallel to the layer orientation except for PLA/1GNPs. PLA/1GNPs fracture surface shows the breaking point begin from the sides of the sample going through the centre. The fracture also occurred perpendicular to the layer orientation. Formation of air void are most visible in PLA/1GNPs and lesser for PLA/3GNPs and PLA/5GNPs. The lack of balance in the microstructure arises due to the improper mixing process. To mitigate the presence of air voids during mixing, increasing the concentration of the plastic solution is suggested. An excess of voids can lead to material weakening and a reduction in mechanical properties. The study provides insights into the mechanical properties of PLA/5GNPs mixtures yields the most favourable outcome compared to other compositions.

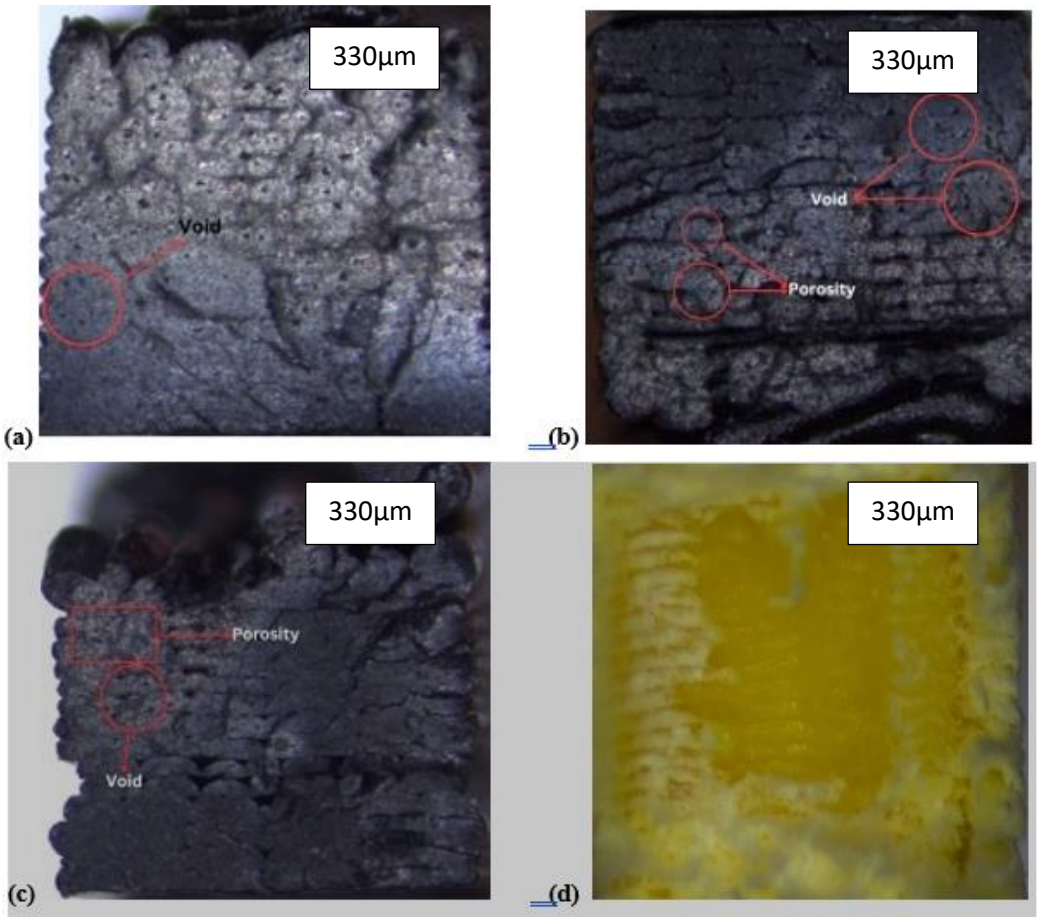

Fig. 9. Optical microscope tensile test sample a) PLA/1GNPs b) PLA/3GNPs c) PLA/5GNPs d) Neat PLA

Surfaces of the samples illustrated in Figure 10 shows PLA/1GNPs is rougher compared to PLA/3GNPs and PLA/5GNPs, respectively. Using optical images, the porosity fractions of the printed samples were quantitatively analysed. Samples with low graphene nanoplatelets weight percentage exhibited greater porosity. Porosity fraction has a negative impact on mechanical properties where

an increase of graphene fraction improves mechanical properties. Consequently, when printed samples with differing graphene fractions were compared, samples with a higher fraction of graphene exhibited a greater mechanical strength.

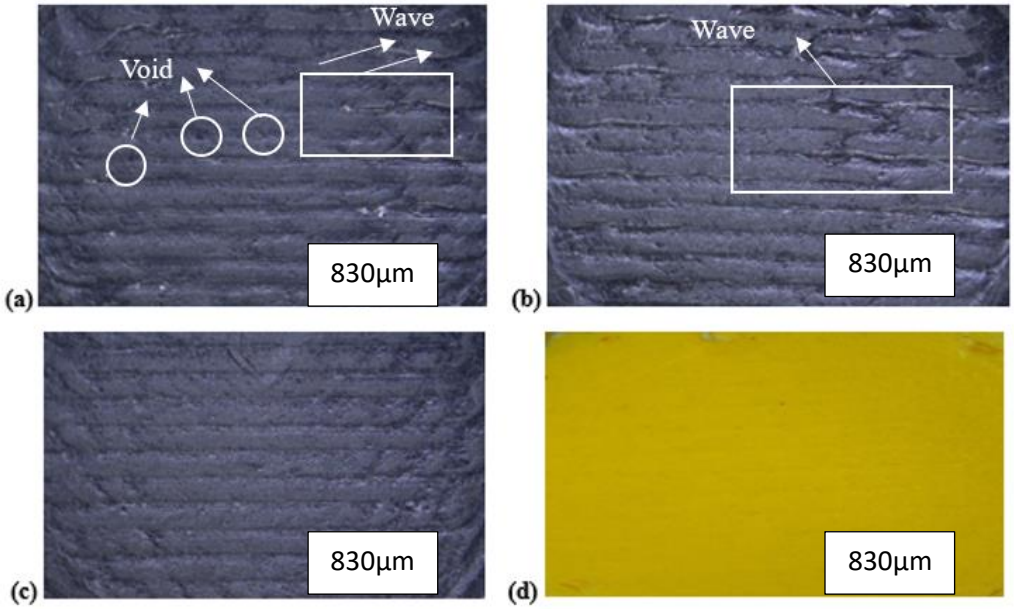

Fig. 10. Optical microscope compression test sample (a) PLA /1GNPs (b) PLA/3GNPs (c) PLA/5GNPs (d) Neat PLA

Figure 11 show the interlayer gaps and profile irregularity that result from poor size consistency in 3D printing. Imperfections include irregularities including roughness, waves and changes in layer thickness. Weak interlayer connections, insufficient material flow and inadequate printing parameters setting can all be attributes for these irregularities. When there is insufficient fusion or bonding between layers, gaps and voids are developed in printed sample structures, which are known as gap interlayer defects. These defects could result from improper material deposition, insufficient melting or poor control of temperatures throughout the printing process.

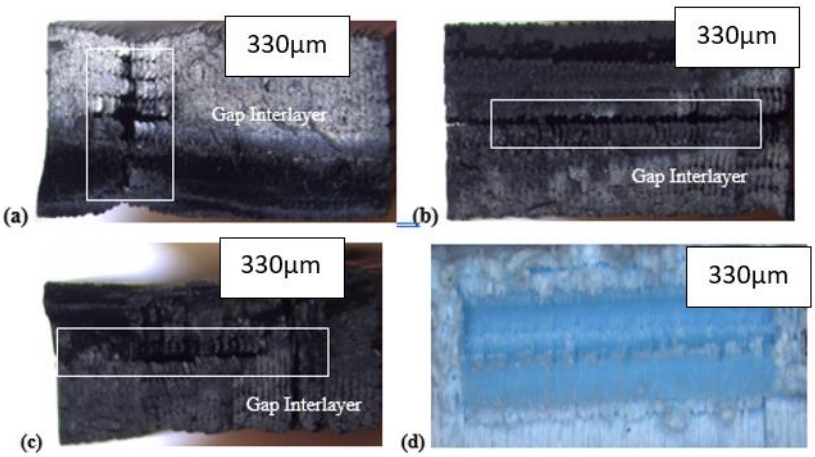

Fig. 11. Optical microscope flexural test sample (a) PLA/1GNPs (b) PLA/3GNPs (c) PLA/5GNPs (d) Neat PLA

4. Conclusion

This paper presents the fabrication and characterization of 3D printed PLA/GNPs biopolymer composites, with a focus on manipulating the GNPs weight percentage to enhance their physical, mechanical and morphological properties. By using a double planetary mixer for biopolymer preparation, we have successfully improved material properties, offering a cost-effective solution for small 3D printing technology-based companies to meet market demands and innovate customized material combinations. Density measurements show that the PLA/GNP composites maintain good dimensional accuracy, making them promising candidates for various applications.

The comprehensive analysis of PLA composites reinforced with GNPs at different weight percentages (1%, 3% and 5%) reveals remarkable improvements in mechanical properties. Among the compositions, PLA/1GNPs stand out, exhibiting the highest average Tensile stress at Tensile strength (74.31 MPa), outperforming PLA/3GNPs (71.63 MPa) and PLA/5GNPs (65.45 MPa). The Modulus (Automatic Young's) also shows significant enhancement, reaching a peak value of 1237.62 MPa for PLA/1GNPs. Furthermore, PLA/1GNPs displays the highest average Modulus and Compressive stress at Maximum Force, with values of 4930.29 MPa and 119.496 MPa, respectively.

The incorporation of 1% GNPs consistently leads to the most significant improvements in mechanical properties, making PLA/1GNPs the standout composition among the different weight percentages. These composites exhibit substantial enhancements in stiffness, tensile strength and compressive behaviour, making them ideal for applications requiring high strength-to-weight ratios and superior mechanical performance. Quantitative conclusion made is supported by qualitative proof in microstructure study where PLA/1GNPs morphology shows the best surface with less interlayer gap and presence of void.

In conclusion, the addition of GNPs to PLA results in notable improvements in mechanical properties, paving the way for the development of advanced composite materials with unique performance characteristics. This study advances material science and engineering, offering exciting possibilities for the development of high-performance, sustainable materials for a wide range of industrial applications. The findings presented in this paper contribute to the growing body of knowledge on nanocomposite materials and provide valuable insights for researchers and industries exploring innovative materials for various applications.

Acknowledgements

The authors would like to be obliged to Faculty of Mechanical and Automotive Engineering Technology (FTKMA), Universiti Malaysia Pahang (UMP) for providing laboratory facilities. Universiti Malaysia Pahang for providing both laboratory facilities and financial assistance under project grant no. RDU223306.

References

[1] Vickram, A. S., A. Saravanan, P. Senthil Kumar, P. Thamarai, S. Yasodha, G. Jamuna, and Gayathri Rangasamy. "An integrated approach to the sustainable development and production of biofuel from biopolymers and algal biomass derived from wastewater." *Fuel* 349 (2023): 128691. https://doi.org/10.1016/j.fuel.2023.128691

[2] Phiri, Resego, Sanjay Mavinkere Rangappa, Suchart Siengchin, Oluseyi Philip Oladijo, and Hom Nath Dhakal. "Development of sustainable biopolymer-based composites for lightweight applications from agricultural waste biomass: A review." *Advanced Industrial and Engineering Polymer Research* (2023). https://doi.org/10.1016/j.aiepr.2023.04.004

[3] Babaremu, Kunle, Oluseyi P. Oladijo, and Esther Akinlabi. "Biopolymers: A suitable replacement for plastics in product packaging." *Advanced Industrial and Engineering Polymer Research* 6, no. 4 (2023): 333-340. https://doi.org/10.1016/j.aiepr.2023.01.001

[4] Udayakumar, Gowthama Prabu, Subbulakshmi Muthusamy, Bharathi Selvaganesh, N. Sivarajasekar, Krishnamoorthy Rambabu, Fawzi Banat, Selvaraju Sivamani, Nallusamy Sivakumar, Ahmad Hosseini-Bandegharaei, and Pau Loke Show. "Biopolymers and composites: Properties, characterization and their applications in food, medical and pharmaceutical industries." *Journal of Environmental Chemical Engineering* 9, no. 4 (2021): 105322. https://doi.org/10.1016/j.jece.2021.105322

[5] Gauss, Christian, Kim Pickering, Maxime Barbier, and Tim Miller. "Additive manufacturing of hygromorphic structures using regenerated cellulose/PLA biocomposites." *Materials Today: Proceedings* (2023). https://doi.org/10.1016/j.matpr.2023.04.227

[6] Bakhshi, Rasoul, Meysam Mohammadi-Zerankeshi, Melika Mehrabi-Dehdezi, Reza Alizadeh, Sheyda Labbaf, and Parvin Abachi. "Additive manufacturing of PLA-Mg composite scaffolds for hard tissue engineering applications." *Journal of the Mechanical Behavior of Biomedical Materials* 138 (2023): 105655. https://doi.org/10.1016/j.jmbbm.2023.105655

[7] Zerankeshi, Meysam Mohammadi, Sayed Shahab Sayedain, Mobina Tavangarifard, and Reza Alizadeh. "Developing a novel technique for the fabrication of PLA-graphite composite filaments using FDM 3D printing process." *Ceramics International* 48, no. 21 (2022): 31850-31858. https://doi.org/10.1016/j.ceramint.2022.07.117

[8] De Maio, Flavio, Enrico Rosa, Giordano Perini, Alberto Augello, Benedetta Niccolini, Francesca Ciaiola, Giulia Santarelli *et al.,* "3D-printed graphene polylactic acid devices resistant to SARS-CoV-2: Sunlight-mediated sterilization of additive manufactured objects." *Carbon* 194 (2022): 34-41. https://doi.org/10.1016/j.carbon.2022.03.036

[9] João, Afonso F., Raquel G. Rocha, Tiago A. Matias, Eduardo M. Richter, João Flávio S. Petruci, and Rodrigo AA Muñoz. "3D-printing in forensic electrochemistry: Atropine determination in beverages using an additively manufactured graphene-polylactic acid electrode." *Microchemical Journal* 167 (2021): 106324. https://doi.org/10.1016/j.microc.2021.106324

[10] Podgórski, Rafał, Michał Wojasiński, Edyta Trepkowska-Mejer, and Tomasz Ciach. "A simple and fast method for screening production of polymer-ceramic filaments for bone implant printing using commercial fused deposition modelling 3D printers." *Biomaterials Advances* 146 (2023): 213317. https://doi.org/10.1016/j.bioadv.2023.213317

[11] Huang, Wei, Jianhui Zhang, Vikaramjeet Singh, Lulu Xu, Prasenjit Kabi, Eral Bele, and Manish K. Tiwari. "Digital light 3D printing of a polymer composite featuring robustness, self-healing, recyclability and tailorable mechanical properties." *Additive Manufacturing* 61 (2023): 103343. https://doi.org/10.1016/j.addma.2022.103343

[12] Alarifi, Ibrahim M. "Mechanical properties and numerical simulation of FDM 3D printed PETG/carbon composite unit structures." *journal of materials research and technology* 23 (2023): 656-669. https://doi.org/10.1016/j.jmrt.2023.01.043

[13] Chen, Fang, Cheng Yang, Zimo An, Xinxing Zhang, Tao Zhou, and Ning Chen. "Direct-ink-writing of multistage-pore structured energy collector with ultrahigh ceramic content and toughness." *Materials & Design* 217 (2022): 110652. https://doi.org/10.1016/j.matdes.2022.110652

[14] Rajan, Kumaresan, Mahendran Samykano, Kumaran Kadirgama, Wan Sharuzi Wan Harun, and Md Mustafizur Rahman. "Fused deposition modeling: process, materials, parameters, properties, and applications." *The International Journal of Advanced Manufacturing Technology* 120, no. 3 (2022): 1531-1570. https://doi.org/10.1007/s00170-022-08860-7

[15] Penumakala, Pavan Kumar, Jose Santo, and Alen Thomas. "A critical review on the fused deposition modeling of thermoplastic polymer composites." *Composites Part B: Engineering* 201 (2020): 108336. https://doi.org/10.1016/j.compositesb.2020.108336

[16] Kim, Hang-Gyeom, Sugato Hajra, Dongik Oh, Namjung Kim, and Hoe Joon Kim. "Additive manufacturing of high-performance carbon-composites: An integrated multi-axis pressure and temperature monitoring sensor." *Composites Part B: Engineering* 222 (2021): 109079. https://doi.org/10.1016/j.compositesb.2021.109079

[17] Korey, Matthew, Mitchell L. Rencheck, Halil Tekinalp, Sanjita Wasti, Peter Wang, Samarthya Bhagia, Rebecca Walker *et al.,* "Recycling polymer composite granulate/regrind using big area additive manufacturing." *Composites Part B: Engineering* 256 (2023): 110652. https://doi.org/10.1016/j.compositesb.2023.110652

[18] Thomas, Akshay J., Eduardo Barocio, Ilias Bilionis, and R. Byron Pipes. "Bayesian inference of fiber orientation and polymer properties in short fiber-reinforced polymer composites." *Composites Science and Technology* 228 (2022): 109630. https://doi.org/10.1016/j.compscitech.2022.109630

[19] Li, Lijun, Wenyao Liu, Yubo Wang, and Zhiyong Zhao. "Mechanical performance and damage monitoring of CFRP thermoplastic laminates with an open hole repaired by 3D printed patches." *Composite Structures* 303 (2023): 116308. https://doi.org/10.1016/j.compstruct.2022.116308

[20] Vatandaş, Bahri Barış, Altuğ Uşun, Nuri Yıldız, Cemaleddin Şimşek, Ömer Necati Cora, Mustafa Aslan, and Recep Gümrük. "Additive manufacturing of PEEK-based continuous fiber reinforced thermoplastic composites with high

mechanical properties." *Composites Part A: Applied Science and Manufacturing* 167 (2023): 107434. https://doi.org/10.1016/j.compositesa.2023.107434

[21] Zhang, Hang, and Wei-fu Sun. "Mechanical properties and failure behavior of 3D printed thermoplastic composites using continuous basalt fiber under high-volume fraction." *Defence Technology* 27 (2023): 237-250. https://doi.org/10.1016/j.dt.2022.07.010

[22] Kim, Yeon Jae, Deok-Ho Kim, Jong Seob Choi, and Jin-Heong Yim. "A multi-functional ammonia gas and strain sensor with 3D-printed thermoplastic polyurethane-polypyrrole composites." *Polymer* 240 (2022): 124490. https://doi.org/10.1016/j.polymer.2021.124490

[23] Gong, Zhou, Jiarong Huang, Jianfeng Fan, Xiaoqing Chen, Hui Wang, and Yukun Chen. "A super-toughened poly (lactic acid)-based thermoplastic vulcanizate through incorporating modified SiO2 nanoparticles." *Composites Science and Technology* 226 (2022): 109558. https://doi.org/10.1016/j.compscitech.2022.109558

[24] Doner, Sami, Rakesh Paswan, and Sumanta Das. "The influence of metallic particulate inclusions on the mechanical and thermal performance of 3D printable acrylonitrile-butadiene-styrene/thermoplastic polyurethane fused polymer blends." *Materials Today Communications* 35 (2023): 106111. https://doi.org/10.1016/j.mtcomm.2023.106111

[25] Wang, Zhaogui, and Douglas E. Smith. "Numerical analysis of screw swirling effects on fiber orientation in large area additive manufacturing polymer composite deposition." *Composites Part B: Engineering* 177 (2019): 107284. https://doi.org/10.1016/j.compositesb.2019.107284

[26] El Moumen, Ahmed, Mostapha Tarfaoui, and Khalid Lafdi. "Additive manufacturing of polymer composites: Processing and modeling approaches." *Composites Part B: Engineering* 171 (2019): 166-182. https://doi.org/10.1016/j.compositesb.2019.04.029

[27] Eda, Goki, and Manish Chhowalla. "Graphene-based composite thin films for electronics." *Nano letters* 9, no. 2 (2009): 814-818. https://doi.org/10.1021/nl8035367

[28] Markandan, Kalaimani, Pawan Kumar Kanaujia, Jain Palash Abhineet, Xiu Yun Yap, Chee Lip Gan, and Chang Quan Lai. "Improvements in the modulus and strength of multi-dimensional hybrid composites through synergistic reinforcement between 1D fiber and 0D particle fillers." *Journal of Materials Science* 56, no. 27 (2021): 15162-15179. https://doi.org/10.1007/s10853-021-06277-3

[29] Markandan, Kalaimani, and Chang Quan Lai. "Fabrication, properties and applications of polymer composites additively manufactured with filler alignment control: A review." *Composites Part B: Engineering* 256 (2023): 110661. https://doi.org/10.1016/j.compositesb.2023.110661

[30] Long, Jiecai, Can Wang, Jingzhen Zhu, Xiaobin Zhan, Zhibin Sun, Baojun Shen, and Xiwen Li. "Discrete element simulation for mixing performances and power consumption in a twin-blade planetary mixer with non-cohesive particles." *Advanced Powder Technology* 33, no. 2 (2022): 103437. https://doi.org/10.1016/j.apt.2022.103437

[31] Long, Jiecai, Yu He, Xiaobin Zhan, Zhibin Sun, Baojun Shen, and Xiwen Li. "Study of kneading pressure and power consumption in a twin-blade planetary mixer for mixing highly viscous fluids." *Chemical Engineering Science* 241 (2021): 116723. https://doi.org/10.1016/j.ces.2021.116723

[32] Sinnott, M. D., S. M. Harrison, and P. W. Cleary. "A particle-based modelling approach to food processing operations." *Food and Bioproducts Processing* 127 (2021): 14-57. https://doi.org/10.1016/j.fbp.2021.02.006

[33] White, Justin, Christopher Tenore, Austin Pavich, Ryan Scherzer, and Stephen Stagon. "Environmentally benign metallization of material extrusion technology 3D printed acrylonitrile butadiene styrene parts using physical vapor deposition." *Additive Manufacturing* 22 (2018): 279-285. https://doi.org/10.1016/j.addma.2018.05.016